Calorimetric Study of Adsorption of Alkanes in High-Silica Zeolites

Scott Savitz, Flor Siperstein, Raymond J. Gorte, and Alan L. Myers

Department of Chemical Engineering, University of Pennsylvania, Philadelphia, Pennsylvania 19104-6393

Received: April 13, 1998; In Final Form: June 23, 1998

Isosteric heats and adsorption isotherms were measured for combinations of three alkanes (methane, ethane, propane) on a series of six high-silica zeolites (TON, MTW, UTD-1, MFI, FER, FAU). Three of these zeolites (TON, MTW, UTD-1) have one-dimensional channels, two (MFI, FER) have two-dimensional intersecting channels, and FAU has spherical cavities. Since the adsorbate molecules are nonpolar and the zeolites possess a high Si/Al ratio, electrostatic energies are small in comparison to van der Waals energies. Heats of adsorption of methane at the limit of zero coverage are 27.2, 20.9, and 14.2 kJ/mol in TON, MTW, and UTD-1, respectively. This homologous series of zeolites has one-dimensional channels composed of 10-, 12-, and 14-membered rings of average effective diameter 5.0, 5.9, and 8.8 Å, respectively. Short-range gas−solid interactions between spherical methane molecules and the oxygen atoms composing the pore walls are explained by a smoothed integration of the Lennard−Jones 12-6 potential for cylindrical pores.

Introduction

Nonbonding interactions between adsorbate molecules and zeolites consist of two principal types. The first type is long-range electrostatic interactions between adsorbate molecules and ions in the zeolite; the second type is short-range van der Waals (dispersion) interactions between the adsorbate molecules and the zeolitic framework. Electrostatic interactions are highly sensitive to the polarity of the adsorbate molecule and to the type and location of nonframework cations (e.g., Na, Ca, Mg); van der Waals interactions depend on the geometry of the microporous structure of the zeolite and the size and shape of the adsorbate molecules.

Changes in the strength of electrostatic interactions are achieved by changing the silicon-to-aluminum ratio and by ion exchange of the nonframework cations of the zeolite. Dispersion interactions, which depend on the size and shape of the micropores, are less amenable to fine-tuning than the electrostatic interactions.

Gas−solid dispersion interactions can be investigated by comparing zeolitic structures having the same geometry. The most straightforward example is the class of zeolites having one-dimensional channels of different size: TON, MTW, and UTD-1. Other structures such as ferrierite and silicalite have two-dimensional networks of intersecting channels of different size and shape; for these zeolites, dispersion interactions are somewhat more difficult to interpret. The presence of structural defects and residual aluminum may also complicate the interpretation of dispersion forces in high-silica materials.

Previous studies of high-silica zeolites were mainly on MFI and FAU.[1−12] Gases studied in these materials range from simple polar and nonpolar probes (Ar, CH_4, Kr, Xe, N_2, C_2H_4, and CO_2) to long-chain alkanes and aromatics. Other zeolites that have been studied include TON, FER, KFI,[13] and MOR.[14] However, differences in the molecular structure of the probe molecules and the complexity of the pore structures in many of the molecular sieves examined make it difficult to isolate and quantify the effect of geometric factors upon dispersion forces. In the present study, work is focused on a homologous series of nonpolar probe molecules in a homologous series of high-silica zeolites. In all of the systems examined, the dispersion energy dominates and electrostatic interactions are negligible or at least very small relative to dispersion. These results should be useful in establishing accurate force fields for dispersion interactions in computer simulations of adsorption.

2. Experimental Section

Isosteric heats of adsorption and adsorption isotherms were measured for all combinations of three adsorbates (methane, ethane, and propane) and six adsorbents (TON, MTW, UTD-1, MFI, FER, FAU). The structure codes are listed in the Atlas of Zeolite Structure Types.[15] All of these are siliceous zeolites with high Si/Al ratios and relatively few nonframework cations. Data for CH_4 and C_2H_6 on silicalite published previously[6] are included here for completeness.

Materials. Ethane and propane with purities of 99% and 99.5%, respectively, were obtained from Air Products and Chemicals, Inc. Methane (99.99% pure) was obtained from Airco.

The MFI (silicalite) powder used was Linde S115 manufactured by Union Carbide Corp. FER (ferrierite) with a Si/Al ratio of 22 was manufactured by Philadelphia Quartz Corp. UTD-1 was supplied by Ken Balkus and A. Ramsaran at the University of Texas, Dallas.[16] FAU (siliceous faujasite) was prepared by Anthony Cheetham at the University of California, Santa Barbara.[17] TON (ZSM-22) and MTW (ZSM-12) zeolites were synthesized in our laboratory according to published procedures.[18−20] The Si/Al ratios and pore volumes for these zeolites are given in Table 1. Pore volumes were obtained from adsorption isotherms of *n*-hexane at 25 °C assuming that the density of adsorbed *n*-hexane at saturation is equal to its liquid density (0.655 g/cm^3). The vapor pressure of *n*-hexane at 25 °C is 20.2 kPa, but saturation was reached at $P < 3$ kPa. Because of the assumption that liquid hexane completely fills the pores, the pore volumes extracted from the saturation capacity of *n*-hexane are only approximate.

The powder samples were pressed into thin wafers to prevent accumulation of dust. Samples were weighed under ambient

S1089-5647(98)01836-7 CCC: $15.00
Published on Web 08/11/1998

TABLE 1: Si/Al Ratios and Pore Volumes of Zeolites

zeolite	V_p (cm^3/g)	Si/Al ratio
TON	0.069	52
MTW	0.097	140
UTD-1	0.106	∞
FER	0.105	22
MFI	0.173	300
FAU	0.245	∞

conditions, and the dehydrated weights were calculated from separate gravimetric measurements in vacuo.

The degassing procedure for all zeolites was the same. Samples were heated under vacuum from room temperature to 110 °C over a period of 24 h for fresh samples and 12 h for used samples, then the temperature was ramped from 110 °C to 350 °C over a period of 12 h, and finally the temperature was held constant for 12 h.

Apparatus. The combination calorimeter−volumetric apparatus contains a 20 cm^3 cubical Pyrex sample cell encased on five of its six sides by thermopiles. The sample cell encased in thermopiles sits inside an aluminum block which provides a large thermal mass for rapid heat dissipation and small temperature rise. The output signal from the thermopiles, which is proportional to the heat flux, is input to a computer which stores the response curve and performs a numerical integration for the total heat released by adsorption of a known increment of gas. The primary calibration of the calorimeter is based upon the Clapeyron equation applied to a series of adsorption isotherms measured in a separate, high-precision volumetric apparatus for ethane on silicalite; the calibration based on electrical heating was essentially the same but less precise.

The sample cell is connected to a dosing loop and pressure transducer for simultaneous determination of the adsorption isotherm and the heat of adsorption. The amount adsorbed is determined by the volumetric method as the difference between the amount of gas admitted and the amount of gas remaining in the dead space of the sample cell at equilibrium. Helium at room temperature was used to determine the dead space inside the sample cell for each zeolite sample.

The reversibility of the measurements was verified by comparing points obtained by adsorption and desorption of the sample. The experimental results were checked for reproducibility by repeating the experiment for different samples of the same adsorbent.

3. Results of Experiment

The series of zeolites TON, MTW, and UTD-1 is especially interesting because all three have one-dimensional straight channels of increasing ring size, as shown in Table 2. Isosteric heats of adsorption for this series are shown on Figures 1−3 for CH_4, C_2H_6, and C_3H_8, respectively. The most prominent feature of these results is the decrease in heat of adsorption with increasing pore size. However, a more subtle competition between energetic heterogeneity of gas−solid interactions and cooperative gas−gas interactions is evident in the heat profiles. Energetic heterogeneity generates a heat of adsorption which decreases with loading; cooperative interactions generate a heat of adsorption which increases with loading. As expected, the relative strength of cooperative interactions increases in the order CH_4, C_2H_6, C_3H_8 for a given adsorbent and in the order of increasing pore size for a given adsorbate.

Isosteric heats of adsorption are reported for FER, MFI, and FAU in Figures 4−6, respectively. The trend of lower heats

TABLE 2: Cavity Dimensions of Zeolites[a]

zeolite	type of cavity	no. of members in ring	cavity
TON (ZSM-22)	1-D cylindrical	10	5.5 × 4.4
MTW (ZSM-12)	1-D cylindrical	12	6.2 × 5.5
UTD-1	1-D cylindrical	14	10.0 × 7.5
FER	2-D cylindrical	8,10	4.8 × 3.5, 5.4 × 4.2
MFI	2-D cylindrical	10,10	5.3 × 5.6, 5.1 × 5.5
FAU	spherical		12.6

[a] The dimensions are the major and minor axes of the elliptical channels. For FER and MFI, dimensions are given for both channels. For FAU, the dimension is the diameter of the supercage. In all cases, the distance is the center-to-center distance between oxygen atoms minus 2.7 Å.

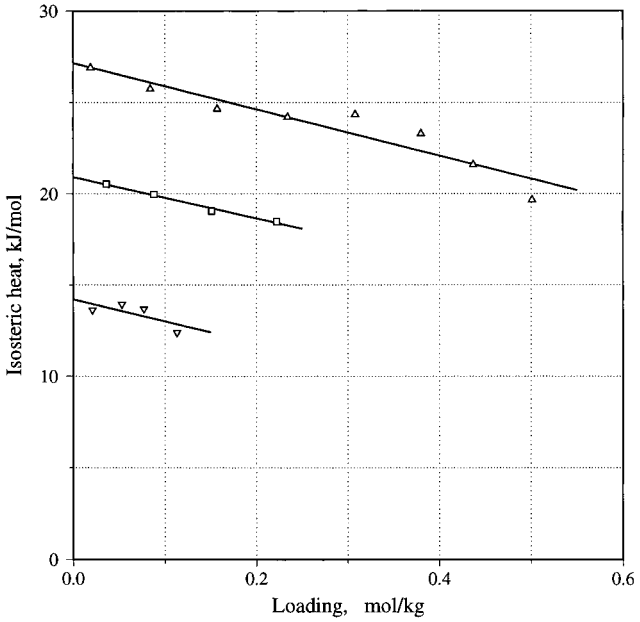

Figure 1. Isosteric heats of adsorption of methane on siliceous materials with one-dimensional channels at 298 K: (△) TON; (□) MTW; (▽) UTD-1.

in larger cavities is apparent in this series of zeolites. Bates et al.[21] showed that for pore openings larger than 5 Å, heats of adsorption decrease as the opening of the pore increases. The subtler competition between energetic heterogeneity and cooperative interactions mentioned previously causes the relative strength of cooperative interactions to increase with pore size.

Isosteric heats are reported in Tables 9−26. Limiting values at zero coverage for the heats of adsorption are listed in Table 3. This is the Boltzman average energy (strictly enthalpy) of a single probe molecule interacting with the walls of the channel.

As shown in Table 4, our heats agree very well with the data of Zhu et al.[9] and the C_3H_8/TON results of Eder and Lercher.[13] All of the published data agree within 5% for CH_4, C_2H_6, and C_3H_8 on MFI. However, there is a variation of ±10% in heats of adsorption reported by different investigators for the other systems.

The one-dimensional straight-channel zeolites TON, MTW, and UTD-1 exhibit a strong decrease in the zero-coverage heat of adsorption with increasing pore size, as expected for dispersion energies. Similarly, the two-dimensional intersecting channels in FER and MFI show a strong decrease in heat of adsorption with increasing pore size. The spherical shape of the supercavities in FAU makes a comparison with the cylindrical channels of the other zeolites problematic, but the heat of adsorption for all the probe molecules is least in FAU.

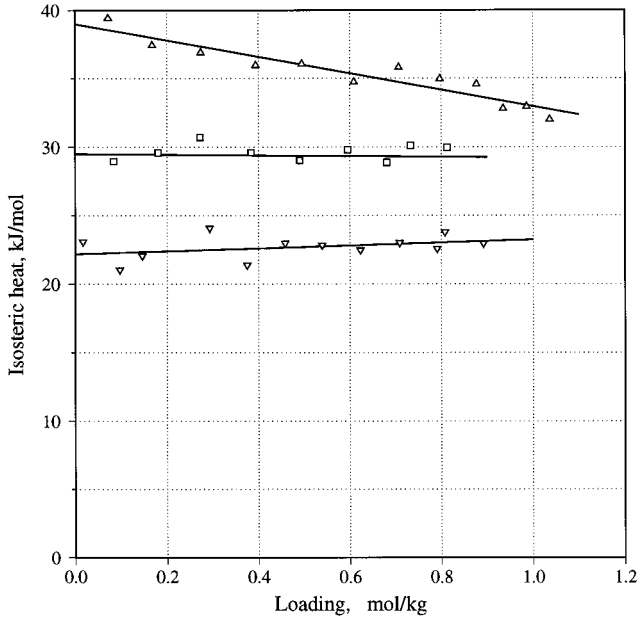

Figure 2. Isosteric heats of adsorption of ethane on siliceous materials with one-dimensional channels at 298 K: (△) TON; (□) MTW; (▽) UTD-1.

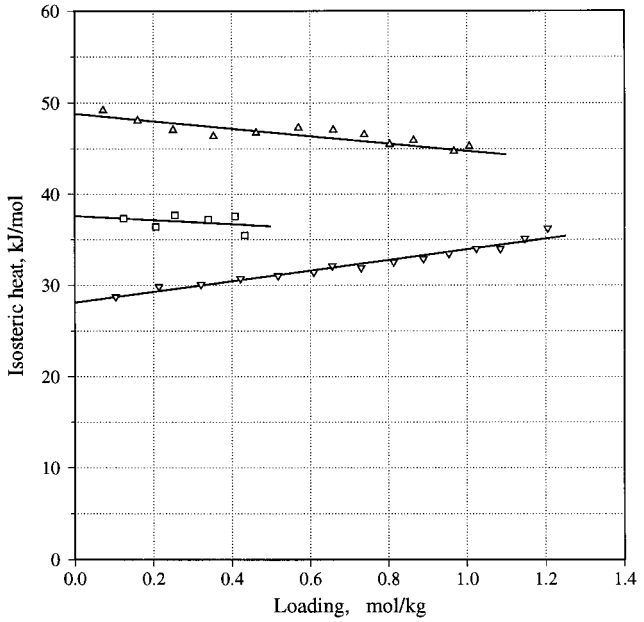

Figure 3. Isosteric heats of adsorption of propane on siliceous materials with one-dimensional channels at 298 K: (△) TON; (□) MTW; (▽) UTD-1.

It is interesting that the increase in heat of adsorption per additional carbon atom in the alkane chain is a strong function of the size of the micropore. It has been reported from experimental measurements[7,8,11,13] and from computer simulations[21−26] that heats of adsorption in MFI increase approximately 10 kJ/mol with each carbon atom in the alkane chain. Table 5 confirms these results: the incremental increase in heat of adsorption per carbon atom is about 10 kJ/mol for MFI but increases in smaller pores (FER) and decreases in larger pores (UTD-1).

Henry's constants calculated from adsorption isotherms measured in a volumetric apparatus are given in Table 6. The adsorption isotherms are reported in Tables 27−37; asterisks identify desorption points taken to check for reversibility.

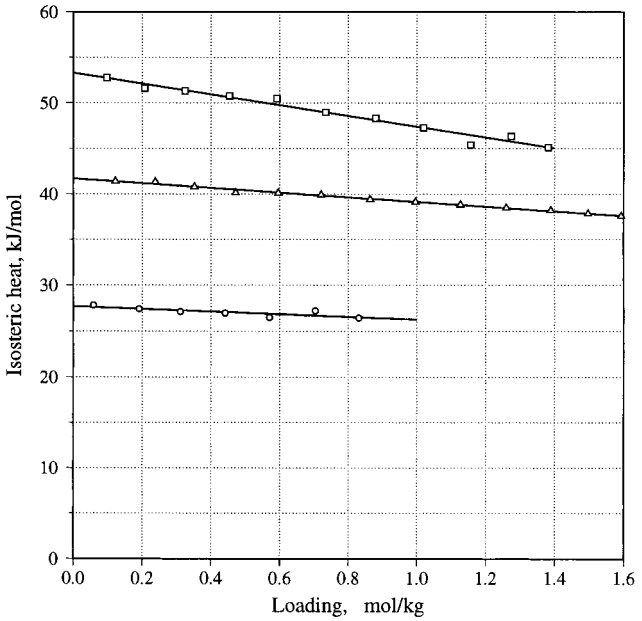

Figure 4. Isosteric heats of adsorption of alkanes on FER at 298 K: (○) methane; (△) ethane; (□) propane.

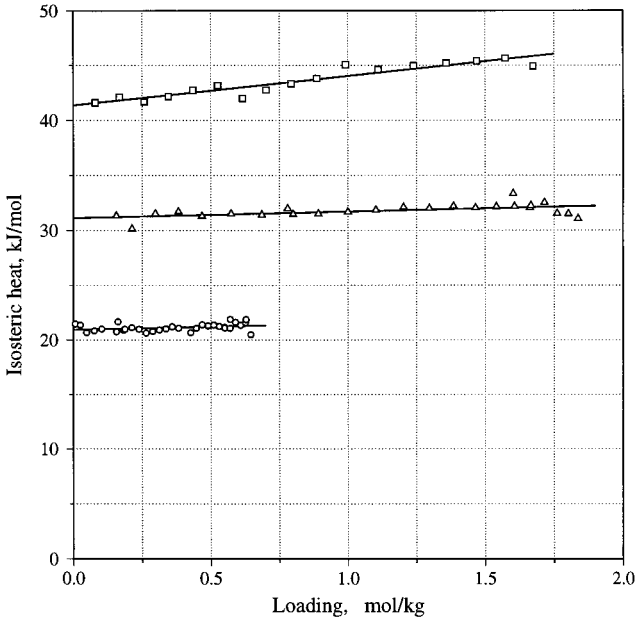

Figure 5. Isosteric heats of adsorption of alkanes on MFI at 298 K: (○) methane; (△) ethane; (□) propane.

4. Discussion and Interpretation of Results

The heats of adsorption obtained for zeolites in one-dimensional channels (TON, MTW, UTD-1) were compared with theoretical calculations based upon the following model: (1) Lennard−Jones 12-6 potential (parameters ϵ_{12} and σ_{12}) for the energy of an adsorbate molecule interacting with a single oxygen atom in the wall of a zeolite. (2) Integration of the potential energy over a single layer of oxygen atoms distributed uniformly in the wall of a cylindrical, one-dimensional pore. The potential energy for this model[27] is

$$E(r) = \frac{5}{2}\pi\epsilon_{1s}\left\{\frac{21}{32}\left(\frac{\sigma_{12}}{R}\right)^{10}\left[\sum_{k=0}^{\infty}\alpha_k\left(\frac{r}{R}\right)^{2k}\right] - \left(\frac{\sigma_{12}}{R}\right)^{4}\left[\sum_{k=0}^{\infty}\beta_k\left(\frac{r}{R}\right)^{2k}\right]\right\} \quad (1)$$

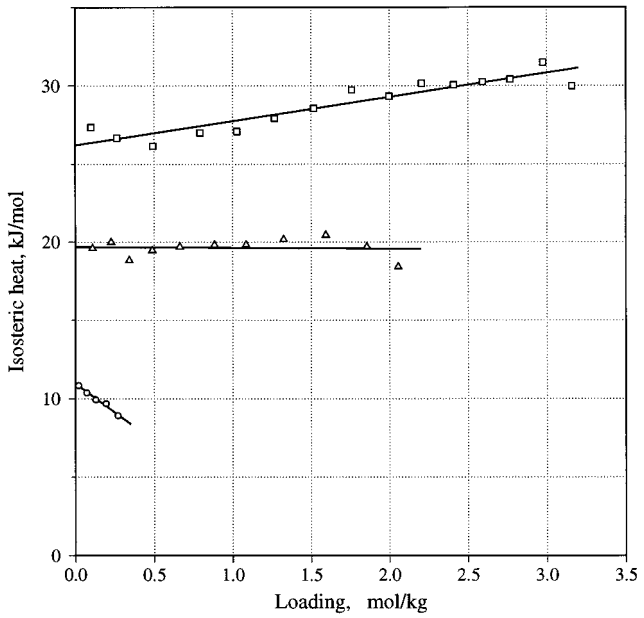

Figure 6. Isosteric heats of adsorption of alkanes on FAU at 298 K: (○) methane; (△) ethane; (□) propane.

TABLE 3: Zero-Coverage Isosteric Heats of Adsorption of Probe Molecules in High-Silica Zeolites at 25 °C

	Q_{st} (kJ/mol)		
zeolite	CH_4	C_2H_6	C_3H_8
FER	27.7	41.7	53.3
TON	27.2	39.0	48.8
MFI	20.9	31.1	41.4
MTW	20.9	29.5	37.6
UTD-1	14.2	22.2	28.1
FAU	11.0	19.7	26.2

TABLE 4: Comparison of Isosteric Heats of Adsorption with Previous Work[a]

		Q_{st} (kJ/mol)	
gas	zeolite	this work	other
CH_4	MFI	20.9	20.5 [8]
			20 [5]
			19 [9]
C_2H_6	MFI	31.1	33 [8]
			30 [5]
			32 [1]
			31 [9]
C_3H_8	MFI	41.4	41 [8]
			41 [5]
			41 [9]
C_2H_6	FAU	19.7	24 [12]
			22 [10]
C_3H_8	FAU	26.2	30 [12]
			28 [10]
C_3H_8	FER	53.3	49 [13]
C_3H_8	TON	48.8	49 [13]

[a] The number given in brackets is the reference number.

where

$$\alpha_k^{1/2} = \frac{\Gamma(-4.5)}{\Gamma(-4.5-k)\Gamma(k+1)} \tag{2}$$

$$\beta_k^{1/2} = \frac{\Gamma(-1.5)}{\Gamma(-1.5-k)\Gamma(k+1)} \tag{3}$$

R is the radius of the cylinder defined by the centers of the oxygen atoms, and r is the distance of the gas molecule from the axis. The gas−solid energy parameter ϵ_{1s} is a function of the surface density of oxygen atoms

$$\epsilon_{1s} = \frac{6}{5}\pi\rho\epsilon_{12}\sigma_{12}^2 \tag{4}$$

where ρ is the number of oxygen atoms per unit area in the wall of the cylinder. ϵ_{1s} is the well depth at the potential-energy minimum in the limit $R \rightarrow \infty$, i.e., the well depth adjacent to a plane surface.

The collision diameter corresponding to $U = 0$ in the Lennard−Jones 12-6 potential is $\sigma_{12} = (2.700 + 3.691)/2 = 3.195$ Å, based upon 2.700 Å for the O atom[15] and 3.691 Å for the CH_4 molecule.[28] The value of the well-depth $\epsilon_{12}/k = 133.33$ K was reported previously.[29] Since the actual channels are elliptical, the average of the major and minor axes (plus 2.7 Å for the diameter of an O atom) was taken as the diameter (D) of the cylindrical channel in the theory so that $R = D/2 = 3.825$, 4.275, and 5.725 for TON, MTW, and UTD-1, respectively.

The area density of oxygen atoms in Table 7 was obtained by counting the oxygen atoms in the channel of a unit cell and dividing by the area of the elliptical channel $(2\pi L[(R_1^2 + R_2^2)/2]^{1/2})$. From eq 4, $\epsilon_{1s}/k = 854$, 917, and 946 K for TON, MTW, and UTD-1, respectively.

Figure 7 shows the potential energies calculated from eq 1 for the three zeolites with one-dimensional channels using the values for ρ, R, σ_{12}, and ϵ_{12} given above. The potential minima $-U/k = 2540$, 2150, and 1540 K for TON, MTW, and UTD-1, respectively. The location of the minimum is at the center of the channel for TON but moves progressively toward the wall for the wider channels in MTW and UTD-1.

The adsorption second virial coefficient for a cylindrical channel is

$$B(T) = \frac{2\pi L}{M}\int_0^R (e^{-E(r)/kT} - 1) r\, dr \tag{5}$$

where L is channel length and M is the mass of a unit cell[15,16] given in Table 7. The −1 in the integrand is required to correct absolute adsorption to excess adsorption and corresponds to the experimental measurement of surface excess (the actual amount adsorbed less the amount present when the surface does not adsorb).

TABLE 5: Incremental Increase in Isosteric Heat Per Methyl or Methylene Group (ΔQ_{st}) Compared to Average Pore Diameter (D) of High-silica Zeolites

zeolite	D (Å)	ΔQ_{st} (kJ/mol)
FER	4.5	12.8
TON	5.0	10.8
MFI	5.4	10.2
MTW	5.9	8.4
UTD-1	8.8	7.0
FAU	12.6	7.6

TABLE 6: Henry's Constants (H) of Alkanes on Siliceous Zeolites

	methane		ethane		propane	
zeolites	H mmol/(g-torr)	T (°C)	H mmol/(g-torr)	T (°C)	H mmol/(g-torr)	T (°C)
FER	0.0026	35.8	0.096	35.8	3.67	36.2
TON	0.00091	35.9	0.0188	35.9		
MFI	0.00084[a]	23.0	0.0164[a]	23.0	0.441	36.3
MTW	0.00054	36.8	0.0124	37.0		
UTD-1	0.00042	36.0	0.0021	36.1	0.0150	36.3

[a] Data from ref 6.

TABLE 7: Structural Properties of Zeolites with One-Dimensional Elliptical Channels

zeolite	g/mol (u.c.)	O atoms/ channel	channels/ u.c.	L (Å)	R_1 (Å)	R_2 (Å)	R (Å)	Area (Å^2)	ρ (O atoms/Å^2)
TON	1442	20	2	5.0	3.55	4.10	3.825	120.5	0.166
MTW	1683	24	1	5.0	4.10	4.45	4.275	134.4	0.179
UTD-1	3846	56	2	8.4	5.10	6.35	5.725	304.0	0.184

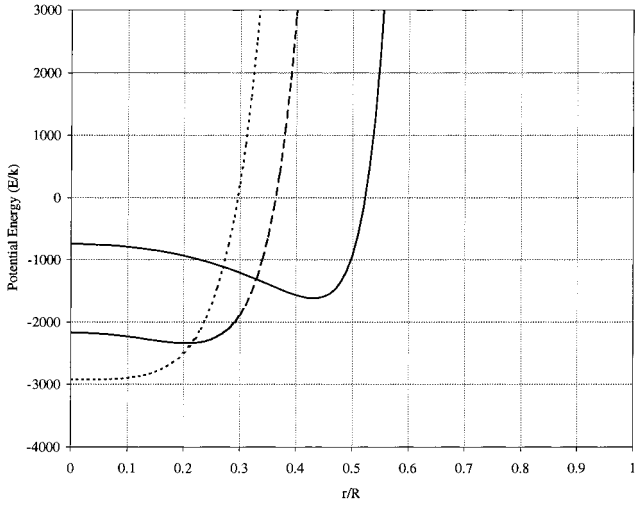

Figure 7. Potential energy of a methane molecule in high-silica zeolites as a function of the dimensionless radius (r/R) of a cylindrical pore: (···) TON; (- - -) MTW; (—) UTD-1.

TABLE 8: Comparison of Theory with Experiment for Henry's Constant and Heat of Adsorption of Methane in High-Silica Zeolites with One-Dimensional Pores

	q_{st} (kJ/mol)		H (mmol/g-Torr)	
zeolites	theory	exp	theory	exp
TON	22.4	27.2	0.00106	0.00091
MTW	19.7	20.9	0.00040	0.00054
UTD-1	14.2	14.2	0.00023	0.00042

TABLE 9: Methane on TON

n (mol/kg)	Q_{st} (kJ/mol)	n (mol/kg)	Q_{st} (kJ/mol)	n (mol/kg)	Q_{st} (kJ/mol)
0.019	26.91	0.234	24.20	0.437	21.60
0.084	25.75	0.308	24.35	0.501	19.66
0.157	24.65	0.380	23.31		

The energy of adsorption at the limit of zero coverage is

$$\bar{E} = \frac{\int_0^R E(r)(e^{-E(r)/kT})r\,dr}{\int_0^R (e^{-E(r)/kT} - 1)r\,dr} \tag{6}$$

The zero-coverage isosteric heat (difference of enthalpies) is

$$q_{st} = -\bar{E} + kT \tag{7}$$

Henry's constants are calculated from the second virial coefficient:

$$H = \frac{B}{kT} \tag{8}$$

Zero-coverage isosteric heats and Henry's constants calculated from eqs 1−8 are summarized in Table 8. The average absolute error is 8% for the heats and 29% for the Henry's constants. This error, although larger than the experimental uncertainty, is surprisingly small considering that published values of Lennard−Jones interaction constants for CH_4−O were used. The 29% error between experimental and calculated Henry's constants is actually in reasonable agreement considering that the Henry's constant is an exponential function of the gas−solid adsorption energy. For example, for CH_4 adsorbed in MTW, an error of only 5% in the potential-well depth corresponds to an error of 45% in the Henry constant. One would expect the neglect of oxygen atoms not located in the walls of the channel to require an artificially large value of ϵ_{12}. Perhaps the neglect of long-range dispersion interactions is compensated by other approximations such as smooth walls and circular instead

TABLE 10: Methane on MTW

n (mol/kg)	Q_{st} (kJ/mol)	n (mol/kg)	Q_{st} (kJ/mol)
0.036	20.54	0.151	19.06
0.088	19.97	0.222	18.49

TABLE 11: Methane on UTD-1

n (mol/kg)	Q_{st} (kJ/mol)	n (mol/kg)	Q_{st} (kJ/mol)
0.021	13.63	0.077	13.69
0.053	13.94	0.113	12.39

TABLE 12: Methane on MFI

n (mol/kg)	Q_{st} (kJ/mol)	n (mol/kg)	Q_{st} (kJ/mol)	n (mol/kg)	Q_{st} (kJ/mol)
0.007	21.46	0.264	20.64	0.530	21.25
0.025	21.36	0.288	20.78	0.550	21.16
0.048	20.66	0.312	20.92	0.550	21.09
0.076	20.84	0.336	21.02	0.569	21.06
0.103	21.01	0.359	21.22	0.570	21.88
0.156	20.75	0.382	21.08	0.589	21.62
0.161	21.67	0.426	20.66	0.608	21.35
0.182	20.88	0.447	21.06	0.626	21.58
0.187	20.98	0.468	21.39	0.628	21.87
0.212	21.14	0.489	21.30	0.645	20.48
0.238	20.98	0.510	21.36		

TABLE 13: Methane on FER

n (mol/kg)	Q_{st} (kJ/mol)	n (mol/kg)	Q_{st} (kJ/mol)	n (mol/kg)	Q_{st} (kJ/mol)
0.059	27.82	0.441	26.97	0.831	26.44
0.191	27.42	0.571	26.50		
0.311	27.11	0.704	27.22		

TABLE 14: Methane on FAU

n (mol/kg)	Q_{st} (kJ/mol)	n (mol/kg)	Q_{st} (kJ/mol)	n (mol/kg)	Q_{st} (kJ/mol)
0.020	10.85	0.129	9.94	0.268	8.92
0.071	10.39	0.193	9.70	0.344	7.25

TABLE 15: Ethane on TON

n (mol/kg)	Q_{st} (kJ/mol)	n (mol/kg)	Q_{st} (kJ/mol)	n (mol/kg)	Q_{st} (kJ/mol)
0.072	39.43	0.495	36.06	0.877	34.57
0.168	37.41	0.609	34.74	0.935	32.79
0.274	36.89	0.707	35.80	0.986	32.93
0.394	35.95	0.797	34.95	1.036	32.00

TABLE 16: Ethane on MTW

n (mol/kg)	Q_{st} (kJ/mol)	n (mol/kg)	Q_{st} (kJ/mol)	n (mol/kg)	Q_{st} (kJ/mol)
0.084	28.98	0.384	29.61	0.681	28.88
0.181	29.60	0.490	29.04	0.733	30.11
0.272	30.73	0.595	29.81	0.813	29.97

TABLE 17: Ethane on UTD-1

n (mol/kg)	Q_{st} (kJ/mol)	n (mol/kg)	Q_{st} (kJ/mol)	n (mol/kg)	Q_{st} (kJ/mol)
0.017	23.08	0.375	21.38	0.709	23.00
0.097	21.04	0.458	22.97	0.791	22.57
0.146	22.05	0.539	22.84	0.808	23.79
0.293	24.08	0.623	22.47	0.892	22.95

TABLE 18: Ethane on MFI

n (mol/kg)	Q_{st} (kJ/mol)	n (mol/kg)	Q_{st} (kJ/mol)	n (mol/kg)	Q_{st} (kJ/mol)
0.156	31.32	0.892	31.50	1.607	32.17
0.213	30.13	1.000	31.67	1.662	32.04
0.298	31.51	1.102	31.84	1.666	32.25
0.382	31.69	1.203	32.10	1.715	32.52
0.468	31.29	1.297	32.00	1.761	31.52
0.574	31.51	1.385	32.19	1.802	31.49
0.686	31.40	1.465	32.04	1.837	31.06
0.780	31.98	1.541	32.14		
0.800	31.46	1.602	33.33		

TABLE 19: Ethane on FER

n (mol/kg)	Q_{st} (kJ/mol)	n (mol/kg)	Q_{st} (kJ/mol)	n (mol/kg)	Q_{st} (kJ/mol)
0.122	41.41	0.721	39.92	1.389	38.19
0.238	41.36	0.864	39.41	1.497	37.83
0.352	40.81	0.996	39.12	1.593	37.55
0.472	40.15	1.127	38.81		
0.596	40.13	1.260	38.47		

TABLE 20: Ethane on FAU

n (mol/kg)	Q_{st} (kJ/mol)	n (mol/kg)	Q_{st} (kJ/mol)	n (mol/kg)	Q_{st} (kJ/mol)
0.109	19.60	0.663	19.70	1.593	20.45
0.227	19.99	0.884	19.82	1.855	19.70
0.342	18.83	1.085	19.83	2.055	18.41
0.488	19.47	1.324	20.18		

TABLE 21: Propane on TON

n (mol/kg)	Q_{st} (kJ/mol)	n (mol/kg)	Q_{st} (kJ/mol)	n (mol/kg)	Q_{st} (kJ/mol)
0.072	49.20	0.462	46.75	0.803	45.49
0.160	48.09	0.570	47.30	0.864	45.92
0.250	47.05	0.659	47.06	0.967	44.72
0.353	46.37	0.738	46.55	1.006	45.25

TABLE 22: Propane on MTW

n (mol/kg)	Q_{st} (kJ/mol)	n (mol/kg)	Q_{st} (kJ/mol)	n (mol/kg)	Q_{st} (kJ/mol)
0.124	37.32	0.255	37.67	0.408	37.55
0.206	36.39	0.340	37.21	0.433	35.49

of elliptical channels. It has been shown[30] that the detailed structure of the micropore becomes important as the pore size decreases.

Figure 8 shows a comparison of theory with the experimental data for all six high-silica zeolites. It is emphasized that we have not fitted any parameters to the experimental data; values of all parameters were obtained either from the structure of the zeolites[15] or from previously published potential parameters.[29] The solid line is the isosteric heat of methane calculated from

TABLE 23: Propane on UTD-1

n (mol/kg)	Q_{st} (kJ/mol)	n (mol/kg)	Q_{st} (kJ/mol)	n (mol/kg)	Q_{st} (kJ/mol)
0.104	28.74	0.609	31.41	0.954	33.43
0.214	29.83	0.656	32.11	1.024	34.00
0.321	30.07	0.730	31.89	1.085	33.95
0.422	30.71	0.813	32.52	1.147	35.09
0.518	31.02	0.889	32.87	1.205	36.22

TABLE 24: Propane on MFI

n (mol/kg)	Q_{st} (kJ/mol)	n (mol/kg)	Q_{st} (kJ/mol)	n (mol/kg)	Q_{st} (kJ/mol)
0.080	41.59	0.616	41.99	1.240	44.96
0.168	42.10	0.701	42.75	1.359	45.19
0.258	41.68	0.793	43.33	1.470	45.40
0.346	42.16	0.887	43.82	1.573	45.65
0.435	42.74	0.992	45.07	1.674	44.91
0.525	43.17	1.111	44.63		

TABLE 25: Propane on FER

n (mol/kg)	Q_{st} (kJ/mol)	n (mol/kg)	Q_{st} (kJ/mol)	n (mol/kg)	Q_{st} (kJ/mol)
0.097	52.77	0.592	50.48	1.157	45.39
0.207	51.60	0.734	48.98	1.274	46.35
0.324	51.32	0.880	48.32	1.382	45.13
0.454	50.77	1.019	47.29		

TABLE 26: Propane on FAU

n (mol/kg)	Q_{st} (kJ/mol)	n (mol/kg)	Q_{st} (kJ/mol)	n (mol/kg)	Q_{st} (kJ/mol)
0.100	27.34	1.267	27.92	2.408	30.05
0.263	26.68	1.516	28.55	2.591	30.25
0.492	26.14	1.759	29.74	2.768	30.42
0.792	27.00	1.997	29.33	2.974	31.47
1.027	27.09	2.204	30.15	3.158	29.99

TABLE 27: Methane on TON at 35.9 °C

P (torr)	n (mmol/g)	P (torr)	n (mmol/g)	P (torr)	n (mmol/g)
12.63	0.0110	108.4	0.0867	338.5	0.2198
21.49	0.0191	133.0	0.1033	390.3	0.2455
31.54	0.0279	152.2	0.1160	407.2	0.2549
36.58	0.0326*	187.3	0.1381	435.2	0.2656
43.71	0.0384	235.1	0.1653	474.3	0.2828
59.25	0.0508	279.0	0.1893*	546.1	0.3144
73.95	0.0616	279.7	0.1898	632.7	0.3461
89.24	0.0731	337.5	0.2189	703.4	0.3722

TABLE 28: Methane on MTW at 36.8 °C

P (torr)	n (mmol/g)	P (torr)	n (mmol/g)	P (torr)	n (mmol/g)
7.32	0.0038	44.01	0.0240	320.0	0.1805
12.53	0.0070*	73.02	0.0386	450.3	0.2322
20.24	0.0107	96.36	0.0505	599.3	0.3084
26.92	0.0147	96.78	0.0556	829.9	0.3856
34.74	0.0196*	141.80	0.0783		
35.08	0.0192	214.40	0.1131		

eqs 6 and 7 as a function of the radius (R) of the pore for an average value $\epsilon_{1s}/k = 907$ K. For the experimental points, the radius of the pore is defined as one-half of the average of the major and minor axes of one-dimensional elliptical pores. For FER and MFI, the radius is defined as the average radius of both elliptical pores; for FAU, the radius is defined as the radius of the supercavity. To conform with the model, these pore diameters are between oxygen-atom centers; the effective diameters in Table 1 are 2.7 Å less to account for the size of the oxygen atoms. The agreement of theory with experiment is much better than expected, considering the simplicity of the

TABLE 29: Methane on UTD-1 at 36.0 °C

P (torr)	*n* (mmol/g)	*P* (torr)	*n* (mmol/g)	*P* (torr)	*n* (mmol/g)
57.98	0.0211	92.50	0.0309	161.2	0.0471
63.77	0.0223	95.19	0.0302		
80.59	0.0266*	134.20	0.0399		

TABLE 30: Methane on FER at 36.0 °C

P (torr)	*n* (mmol/g)	*P* (torr)	*n* (mmol/g)	*P* (torr)	*n* (mmol/g)
5.27	0.0135	88.29	0.1836*	393.6	0.6097
13.65	0.0323	90.40	0.1866	464.3	0.6807
16.21	0.0405*	110.80	0.2234	497.2	0.7111*
22.19	0.0508	111.50	0.2244	547.5	0.7553
29.12	0.0678	141.30	0.2744	563.3	0.7676
33.18	0.0759	172.80	0.3337	688.9	0.8640
41.02	0.0924	219.90	0.4014	799.5	0.9379
54.02	0.1183	271.30	0.4693		
72.91	0.1546	327.90	0.5383		

TABLE 31: Ethane on TON at 35.9 °C

P (torr)	*n* (mmol/g)	*P* (torr)	*n* (mmol/g)	*P* (torr)	*n* (mmol/g)
1.99	0.0362	23.91	0.2656	116.7	0.6337
5.00	0.0812	32.68	0.3250	136.8	0.6747
8.30	0.1223	41.95	0.3780	159.2	0.7133
9.70	0.1385*	52.19	0.4290	190.8	0.7593
10.47	0.1484*	63.89	0.4779	301.0	0.8655
12.58	0.1678	76.96	0.5250	362.8	0.9059
13.43	0.1766*	78.83	0.5322*	408.9	0.9309
14.59	0.1875	89.68	0.5645	479.1	0.9624
16.72	0.2080	95.15	0.5803	569.6	0.9946
18.30	0.2206	112.00	0.6225	676.6	1.0246

TABLE 32: Ethane on MTW at 37.0 °C

P (torr)	*n* (mmol/g)	*P* (torr)	*n* (mmol/g)	*P* (torr)	*n* (mmol/g)
3.48	0.0387	23.94	0.2287*	56.66	0.4423*
8.42	0.0899	32.45	0.2928	70.92	0.5137
15.39	0.1557	35.79	0.3160		
22.77	0.2185	50.38	0.4078		

TABLE 33: Ethane on UTD-1 at 36.1 °C

P (torr)	*n* (mmol/g)	*P* (torr)	*n* (mmol/g)	*P* (torr)	*n* (mmol/g)
33.45	0.0645	118.5	0.2327	354.4	0.6446
47.87	0.0929*	141.3	0.2711	355.8	0.6489
51.99	0.1007	163.8	0.3185	482.9	0.8423
63.17	0.1224	193.6	0.3674	490.8	0.8457
66.36	0.1287	218.9	0.4162	580.0	0.9692
82.60	0.1595	264.4	0.4941	693.8	1.1260
86.45	0.1691	265.9	0.4973*		

model for short-range gas−solid interactions. A detailed atom−atom model should improve the agreement with experiment, especially for the small channels in FER and TON.

5. Conclusions

We studied the adsorption of a homologous series of alkanes (C_1-C_3) on a homologous series of high-silica zeolites with straight one-dimensional channels (TON, MTW, UTD-1). The zero-coverage heats of adsorption are inversely proportional to the pore diameter and agree approximately with a smoothed integration for short-range van der Waals interactions. Heats of adsorption of high-silica zeolites with two-dimensional intersecting channels (FER, MFI) and spherical supercages (FAU) also agree with the model. The incremental heat of adsorption per alkane carbon atom is about 10 kJ/mol for MFI but varies between 8 and 13 kJ/mol depending on the pore size.

TABLE 34: Ethane on FER at 35.8 °C

P (torr)	*n* (mmol/g)	*P* (torr)	*n* (mmol/g)	*P* (torr)	*n* (mmol/g)
0.50	0.0438	25.90	0.8978*	46.68	1.1343
1.51	0.1307	27.46	0.9121	47.00	1.1347
3.39	0.2470	28.90	0.9372*	56.25	1.2058
6.21	0.3862	31.81	0.9808*	60.51	1.2361
10.61	0.5502	34.75	1.0163	73.99	1.3123
15.36	0.6840*	36.27	1.0258	88.29	1.3779
17.61	0.7345	37.55	1.0435		
21.03	0.8058	40.97	1.0805*		

TABLE 35: Propane on UTD-1 at 36.3 °C

P (torr)	*n* (mmol/g)	*P* (torr)	*n* (mmol/g)	*P* (torr)	*n* (mmol/g)
7.21	0.1053	18.05	0.2700*	27.10	0.4046
15.11	0.2225	23.39	0.3468	39.43	0.5713

TABLE 36: Propane on MFI at 36.3 °C

P (torr)	*n* (mmol/g)	*P* (torr)	*n* (mmol/g)	*P* (torr)	*n* (mmol/g)
0.19	0.0801	1.96	0.6090*	10.04	2.0292
0.37	0.1522	2.45	0.7668	10.49	2.0691
0.60	0.2368	2.54	0.7886	13.86	2.3353
0.72	0.2760*	2.73	0.8527	16.01	2.4558
1.03	0.3825	3.81	1.0999*	27.50	2.8704
1.03	0.3261*	3.94	1.1201	57.24	3.2460
1.20	0.4477	5.93	1.5016	224.50	3.7043
1.62	0.5233	6.48	1.5841*	472.50	3.8584
1.65	0.5007*	7.15	1.6948	756.20	3.9584
1.81	0.6437	7.52	1.7245		

TABLE 37: Propane on FER at 36.2 °C

P (torr)	*n* (mmol/g)	*P* (torr)	*n* (mmol/g)	*P* (torr)	*n* (mmol/g)
0.03	0.0769	1.23	1.8791	95.45	5.9847
0.11	0.3362	1.41	2.0354*	251.40	6.4155
0.23	0.6391	1.82	2.3390	337.90	6.5045*
0.25	0.6768	2.31	2.6066	443.90	6.5853
0.36	0.8989*	3.97	3.2678	577.80	6.6577
0.41	0.9890	6.13	3.7813	858.10	6.7542
0.54	1.1958	15.48	4.7580		
0.79	1.5373	46.24	5.6104		

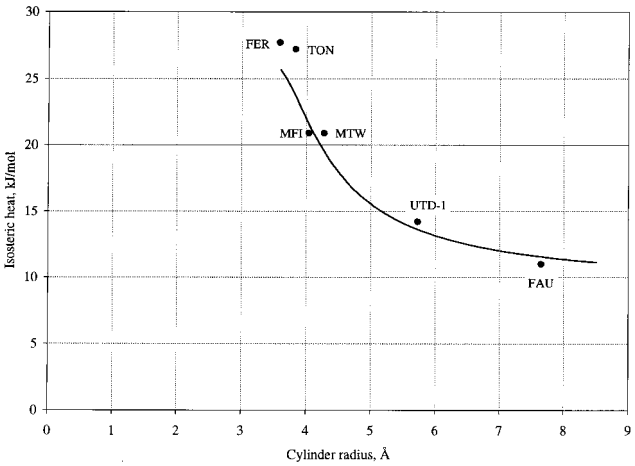

Figure 8. Comparison of theory with experiment for heat of adsorption of methane in high-silica zeolites at 298 K. Solid line calculated from eqs 1−4, 6, and 7 with $\epsilon_{1s}/k = 907$ K and $\sigma = 3.195$ Å. Experimental points are from Table 3.

Acknowledgment. Support was provided by NSF CTS-96-10030. We also thank D.H. Olson, who supplied the FER and TON samples, and Ken Balkus, who supplied the UTD-1 sample.

References and Notes

(1) Thamm, H. *Zeolites* **1987,** *7*, 341.
(2) Abdul-Rehman, H. B.; Hasanain, M. A.; Loughlin, K. F. *Ind. Eng. Chem. Res.* **1990**, *29*, 1525.
(3) Golden, T. C.; Sircar, S. *J. Colloid Interface Sci*. **1994**, *162*, 182.
(4) Otto, K.; Montreuil, C. N.; Todor, O.; McCabe, R. W.; Gandhi, H. S. *Ind. Eng. Chem. Res.* **1991**, *30* (10), 2333.
(5) Hufton J. R.; Danner, R. P. *AIChE J.* **1993**, *39* (6), 954.
(6) Dunne, J. A.; Mariwala, R.; Rao, M.; Sircar, S.; Gorte, R. J.; Myers, A. L. *Langmuir* **1996**, *12*, 5888.
(7) Sun, M. S.; Talu, O.; Shah, D. B. *J. Phys. Chem.* **1996**, *100*, 17276.
(8) Sun, M. S.; Shah, D. B.; Xu, H. H.; Talu, O. *J. Phys. Chem. B* **1998**, *102*, 1466.
(9) Zhu, W.; van de Graaf, J. M.; van den Broeke, L. J. P.; Kapteijn, F.; Moulijn, J. A. *Ind. Eng. Chem. Res.* **1998,** *37* (5) 1934.
(10) Stach, H.; Lohse, U.; Thamm, H.; Schirmer, W. *Zeolites* **1986**, *6*, 74.
(11) Stach, H.; Fiedler, K.; Jänchen J. *Pure Appl. Chem.* **1993**, *65* (10), 2193.
(12) Hampson, J. A.; Rees, L. V. C. *J. Chem. Soc., Faraday Trans.* **1993**, *89* (16), 3169.
(13) Eder, F.; Lercher, J. A. *J. Phys. Chem. B* **1997,** *101*, 1273.
(14) Triebe, R. W.; Tezel, F. H.; Khulbe, K. C. *Gas Sep. Purif.* **1996**, *10* (1), 81.
(15) Olson, D. H.; Meier, W. M. *Atlas of Zeolite Structure Types*, 3rd ed.; Butterworth-Heinemann: London, 1992.
(16) Lobo, R. F.; Tsapatsis, M.; Freyhardt, C. C.; Khodabandeh, S.; Wagner, P.; Chen, C. Y.; Balkus, K. J.; Zones, S. I.; Davis, M. E. *J. Am. Chem. Soc.* **1997**, *119*, 8474.
(17) Milton, R. M. U.S. Patent 2,882,244, 1959.
(18) Kofke, T. J. G.; Gorte, R. J.; Kokotailo, G. T.; Farneth, W. E. *J. Catal.* **1989**, *115*, 265.
(19) Rosinski, E. J.; Rubin, M. K. U.S. Patent 3,832,449, 1974**.** Givens, E. N.; Plank, C. J.; Rosinski, E. J. *U.S. Patent 4,052,472*, 1977.
(20) Valyocsik, E. W. U.S. Patent 4,481,177, 1984.
(21) Bates, S. P.; van Well, W. J. M.; van Santen, R. A.; Smit, B. *J. Am. Chem. Soc.* **1996**, *118*, 6753.
(22) Maginn, E. J.; Bell, A. T.; Theodorou, D. N. *J. Phys. Chem.* **1995**, *99*, 2057.
(23) Smit, B.; Siepmann, J. I. *J. Phys. Chem.* **1994**, *98*, 8442.
(24) Bates, S. P.; van Well, W. J. M.; van Santen, R. A.; Smit, B. *J. Phys. Chem*. **1996**, *100*, 17573.
(25) Smit, B. *J. Phys. Chem.* **1995**, *99*, 5597.
(26) June, R. L.; Bell, A. T.; Theodorou, D. N. *J. Phys. Chem.* **1990**, *94*, 1508.
(27) Everett, D. H.; Powl, J. C. *J. Chem. Soc., Faraday Trans. 1* **1976**, *72*, 619.
(28) Prausnitz, J. M.; Myers, A. L. *AIChE J.* **1963**, *9* (1), 5.
(29) Goodbody, S. J.; Watanabe, K.; MacGowan, D.; Walton, J. P. R. B.; Quirke, N. *J. Chem. Soc., Faraday Trans.* **1991**, *87*, 1951.
(30) Curry, J. E.; Cushman, J. H. *Mol. Phys.* **1995,** *85* (1), 173.